Title

Magnetization-prepared spoiled gradient-echo snapshot imaging for efficient measurement of R2-R1ρ in knee cartilage

Journal

Magnetic Resonance in Medicine, 87(2)

ISSN

0740-3194

Authors

Han, Misung
Tibrewala, Radhika
Bahroos, Emma
et al.

Publication Date

2022-02-01

DOI

10.1002/mrm.29024

Peer reviewed

HHS Public Access

Author manuscript

Magn Reson Med. Author manuscript; available in PMC 2022 June 03.

Published in final edited form as:

Magn Reson Med. 2022 February ; 87(2): 733–745. doi:10.1002/mrm.29024.

Magnetization-Prepared Spoiled Gradient-Echo Snapshot Imaging for Efficient Measurement of R_2-$R_{1\rho}$ in Knee Cartilage

Misung Han, PhD[*,1], **Radhika Tibrewala, MS**[1], **Emma Bahroos, MS**[1], **Valentina Pedoia, PhD**[1,2], **Sharmila Majumdar, PhD**[1,2]

[1]Radiology and Biomedical Imaging, University of California, San Francisco, San Francisco, CA, USA

[2]Center for Digital Health Innovation, University of California, San Francisco, San Francisco, CA, USA

Abstract

Purpose: To validate the potential of quantifying R_2-$R_{1\rho}$ using one pair of signals with $T_{1\rho}$ preparation and T_2 preparation incorporated to magnetization-prepared angle-modulated partitioned k-space spoiled gradient-echo snapshots (MAPSS) acquisition and to find an optimal preparation time (T_{prep}) for in vivo knee MRI.

Methods: Bloch equation simulations were first performed to assess the accuracy of quantifying R_2-$R_{1\rho}$ using $T_{1\rho}$- and T_2-prepared signals with an equivalent T_{prep}. For validation of this technique in comparison to the conventional approach that calculates R_2-$R_{1\rho}$ after fitting both T_2 and $T_{1\rho}$, phantom experiments and in vivo validation with five healthy subjects and five osteoarthritis patients were performed at a clinical 3T scanner.

Results: Bloch equation simulations demonstrated that the accuracy of this efficient R_2-$R_{1\rho}$ quantification method and the optimal T_{prep} can be affected by image SNR and tissue relaxation times, but quantification can be closest to the reference with an around 25 ms T_{prep} for knee cartilage. Phantom experiments demonstrated that the proposed method can depict R_2-$R_{1\rho}$ changes with agarose gel concentration. With in vivo data, significant correlation was observed between cartilage R_2-$R_{1\rho}$ measured from the conventional and the proposed methods, and a T_{prep} of 25.6 ms provided the most agreement by Bland-Altman analysis. R_2-$R_{1\rho}$ was significantly lower in patients than in healthy subjects for most cartilage compartments.

Conclusion: As a potential biomarker to indicate cartilage degeneration, R_2-$R_{1\rho}$ can be efficiently measured using one pair of $T_{1\rho}$-prepared and T_2-prepared signals with an optimal T_{prep} considering cartilage relaxation times and image SNR.

Keywords

Knee Cartilage; Quantitative MRI; Relaxation; R_2-$R_{1\rho}$; Osteoarthritis

[*]*Correspondence to:* Misung Han, PhD, Department of Radiology and Biomedical Imaging, University of California at San Francisco, 1700 4th Street, Suite 201, San Francisco CA 94158, USA. Phone: 415-514-9655, misung.han@ucsf.edu.

Introduction

Osteoarthritis (OA) is the most prevalent joint disease associated with pain and disability in middle-aged and older people, and its prevalence is rising due to an aging population and a rise in obesity.[1,2] One distinctive feature of OA is articular cartilage degeneration, which has a progressive, irreversible course, and is associated with pathology of other joint tissues such as subchondral bone, synovial tissue, and meniscus.

Articular cartilage is hyaline cartilage, being composed of a sparse distribution of chondrocytes surrounded by a dense extracellular matrix (ECM). ECM is functionally responsible for the biomechanical roles of joints, and primarily comprised of water (65-80%), collagen (15-20%, primarily type II), and proteoglycans (PG) (3-10%).[3-5] Collagen forms a 3D fibrillar network, traps PG and water, and provides structural integrity.[6] PG is a macromolecule consisting of a protein core with bound glycosaminoglycan (GAG) side chains that provide cartilage with unique gel-like property.[5,7] Cartilage can be divided into three layers, superficial, middle, and deep zones, from the articular surface to the subchondral bone, possessing varied collagen fiber ultrastructure and chondrocytes distribution.[8-10] In the superficial zone, the collagen fibers are packed tightly and aligned parallel to the articular surface while the lowest PG content and the highest water content are present. In the middle zone, collagen fibers are less organized with oblique orientations. In the deep zone, collagen fibers are the most organized perpendicular to the articular surface while the highest PG content and the lowest water content are present.

Cartilage degeneration is characterized by alteration of collagen structure, loss of PG, and increase in water content, which usually occur prior to joint morphological changes.[11,12] Many quantitative MRI techniques have shown sensitivity to assess biochemical changes in cartilage. T_2, spin-spin relaxation, is largely attributed by interaction between dipoles in spatially restricted water molecules in fiber collagen network, and can represent collagen structure and hydration.[13-15] $T_{1\rho}$, spin-lattice relaxation in a rotating frame, has been shown to be less affected by dipolar interaction.[16] The sensitivity of $T_{1\rho}$ to PG loss was validated in enzymatically degraded cartilage specimens[17-19] while some studies reported a negligible effect of PG loss with $T_{1\rho}$ in naturally-degenerate cartilage.[20,21] A chemical exchange-dependent saturation transfer (CEST) technique can be also used to indirectly measure GAG content in cartilage by exploiting the exchange between hydroxyl (−OH) protons on GAG and bulk water protons[22,23] although capturing the CEST signal below 3T magnetic field strength can be a challenge.[24]

$T_{1\rho}$ variation with the spin-lock frequency, known as $T_{1\rho}$ (or $R_{1\rho}$ (= $1/T_{1\rho}$)) dispersion, results from a reduction of relaxation due to dipolar effects and chemical exchange at a stronger spin lock field strength.[25,26] Based on experiments using protein gels, which mimic biological tissues, chemical exchange between macromolecules and bulk water was shown to contribute significantly to $T_{1\rho}$ dispersion.[26,27] Furthermore, Duvvuri et al[28] also reported that in cartilage chemical exchange from NH and OH groups to bulk water dominates water $R_{1\rho}$ dispersion in the low frequency range (0 - 1.5 kHz). However, Mlynarick et al[29] and recently Pang et al[30] claimed that dipolar interaction would be the dominant relaxation mechanism at $B_0 \leq 3T$ in cartilage. Even though distinguishing

different relaxation mechanisms is not straightforward, $R_{1\rho}$ difference between two spin-lock frequencies has been suggested as a potential parameter to characterize the dispersion curve, which might reflect alteration in cartilage resulted from reduced dipolar interaction or chemical exchange.[30-32] Russell et al[33] and Pedoia et al[34] demonstrated a composite metric R_2-$R_{1\rho}$, $R_{1\rho}$ difference between 0 Hz and 500 Hz spin lock frequencies, has high correlation with patient clinical outcome and cartilage lesion progression compared to either T_2 or $T_{1\rho}$, respectively.

Magnetization-prepared angle-modulated partitioned k-space spoiled gradient echo snapshots (MAPSS)[35,36] combines magnetization preparation such as $T_{1\rho}$ or T_2 preparation with gradient-echo snapshot 3D acquisition, and $T_{1\rho}$ or T_2 can be quantified after acquiring images at multiple preparation times. With MAPSS, R_2-$R_{1\rho}$ can be derived after quantifying both $T_{1\rho}$ and T_2 separately; however, it requires a long acquisition time. A more efficient approach would be to estimate R_2-$R_{1\rho}$ using one pair of $T_{1\rho}$- and T_2-prepared signals with equivalent preparation times as discussed in Russell et al.[33] In this work, we demonstrated the feasibility of quantifying R_2-$R_{1\rho}$ efficiently in the knee cartilage in a presence of B_0 and B_1 inhomogeneities and background noise using Bloch equation simulations. For validation, a phantom study and an in vivo knee MRI study with healthy subjects and OA patients were performed.

Methods

R_2-$R_{1\rho}$ Quantification Using MAPSS

For the MAPSS sequence, $T_{1\rho}$ or T_2 preparation was followed by 3D RF-spoiled gradient-echo (SPGR) acquisition in a segmented radial centric view ordering during a transient state[35] (Figure 1). $T_{1\rho}$ preparation used the composite RF pulse method proposed by Dixon et al,[37] applying a hard RF pulse with a 135° flip angle and an RF phase same as the spin-locking RF pulse right after the 90° tip-down pulse and right before the 90° tip-up pulse to improve robustness to B_0 variation. In addition, two acquisitions with ± signs of the 90° tip-up pulse and the subtraction of two acquired signals (RF phase cycling) was used to reduce B_1 inhomogeneity effects.[38] The RF phase cycling also reduced errors on $T_{1\rho}$ quantification resulted from T_1 relaxation during multiple view acquisition.[35] T_2 preparation used a Malcolm Levitt (MLEV) train of nonselective composite 90°-180°-90° refocusing pulses to provide robustness to B_0 and B_1 inhomogeneities,[39] and RF phase cycling was also applied. The effective TE (TE_{eff}) for each T_2 preparation was determined considering T_1 and T_2 decay during composite refocusing pulses[39] as follows,

$$TE_{\text{uncorr}} = N^{*}T_{\text{SP}}, \quad [1]$$

$$TE_{\text{eff}} = TE_{\text{uncorr}} - T_{\text{REFOC}} * N^{*}(1 - T_2 / T_1) / 2, \quad [2]$$

where N was the number of the refocusing pulses, T_{RFFOC} was the duration of one composite refocusing pulse, and T_{SP} is the spacing between the two consecutive refocusing pulses. The ratio between T_1 and T_2 in cartilage was assumed[40] to be 34. A chemical

selective fat suppression pulse was applied after either $T_{1\rho}$ or T_2 preparation to provide similar fat suppression quality to acquisitions regardless of magnetization preparation.

As a conventional approach to quantify R_2-$R_{1\rho}$ using MAPSS, signals can be acquired at multiple spin lock times (TSLs) with $T_{1\rho}$ preparation and then acquired at multiple TEs with T_2 preparation. R_2-$R_{1\rho}$ can be then calculated after fitting $T_{1\rho}$ and T_2 respectively. In contrast, an efficient approach can only use one pair of $T_{1\rho}$-prepared signal and T_2-prepared signal with an equivalent preparation time (T_{prep}) for R_2-$R_{1\rho}$ computation. In the absence of B_0 and B_1 inhomogeneities and image noise, $T_{1\rho}$-prepared and T_2-prepared signals with a T_{prep} of T_{prep}, i.e., $S_{1\rho}(T_{prep})$ and $S_2(T_{prep})$, can be expressed as

$$S_{1\rho}(T_{prep}) = S_{1\rho}(0) * \exp(-T_{prep} / T_{1\rho}), \quad [3]$$

$$S_2(T_{prep}) = S_2(0) * \exp(-T_{prep} / T_2). \quad [4]$$

Assuming $S_{1\rho}(0) = S_2(0)$, R_2-$R_{1\rho}$ can then be computed as

$$R_2 - R_{1\rho} = (- \ln(S_2(T_{prep})) + \ln(S_{1\rho}(T_{prep}))) / T_{prep}. \quad [5]$$

To provide $S_2(0)$ as similar as $S_{1\rho}(0)$ with our $T_{1\rho}$ and T_2 preparation schemes (Figure 1), T_{prep} for $T_{1\rho}$ preparation was designated as TSL while T_{prep} for T_2 preparation was designated as TE_{eff}-1.2 ms (the duration of the two 135° hard pulses applied for the composite tip-down and tip-up pulse).

Bloch Equation Simulation

The feasibility of using 2-echo MAPSS to quantify R_2-$R_{1\rho}$ in knee cartilage was first demonstrated by magnetization simulations. Magnetization at the end of $T_{1\rho}$ and T_2 preparation used in MAPSS (shown in Figure 1) was simulated using Bloch equations that describe precession and T_1 and T_2 relaxation. Magnetization evolution during the spin-locking pulse was simulated using precession along the effective spin-locking field accounting for B_0 offset and $T_{1\rho}$ and $T_{2\rho}$ relaxation.[38,41] $T_{2\rho}$ relaxation was simulated assuming $T_{2\rho}$ as the average of the reciprocal of T_1 and T_2[42] though $T_{2\rho}$ relaxation effects had been demonstrated to be negligible with phase-cycled $T_{1\rho}$ preparation.[38] For T_2 preparation, TE_{eff} was varied by changing the number of 180° composite refocusing pulses or the interval between 180° composite pulses.

Noise effects were incorporated as a signal bias on the simulated signal, assuming the signal was measured on the square-root of the sum-of-squares of reconstructed images from sixteen receiver coil elements. Simulated signals with a bias due to noise was calculated supposing its following noncentral chi distribution.[43,44] And then R_2-$R_{1\rho}$ was calculated based on the logarithms of the simulated signals with using equivalent T_{prep}. Simulation was conducted by varying the T_{prep}, noise level, and $T_{1\rho}$ and T_2 relaxation times. B_0 and B_1 inhomogeneities effects were also assessed.

Phantom Study

A phantom experiment was performed using a GE Discovery MR750 scanner (GE Healthcare, Waukesha, WI) and a 16-channel medium GEM flex-coil array (Neo-Coil, Pewaukee, WI). Five cylindrical tubes with agarose gel concentration of 2, 4, 6, 8, 10% (weight/volume) were attached to a small GE loading phantom and used for quantification. Agarose phantoms can provide similar $T_{1\rho}$ and T_2 as biological tissues[45,46] in a presence of exchange between free water and agar (macromolecule).[47] First, 8-echo MAPSS was first performed with TSLs of 0, 12.8, 40, 80 ms, and spin lock frequency of 500 Hz for $T_{1\rho}$ quantification, and TE_{eff} times of 0, 12.8, 25.7, and 51.4 ms for T_2 quantification. To provide the last three TE_{eff} times, the interval between consecutive refocusing pulses (T_{SP}) was 4 ms and the numbers of refocusing pulses were 4, 8 and 16. The fat saturation pulse was turned off. Imaging parameters included were a FOV of 14 x 14 cm^2, 128 x 128 matrix size, 4 mm slice thickness, 24 slices, ±62.5 kHz readout bandwidth, 76 phase-encode lines (views) acquisition per each $T_{1\rho}$ or T_2 preparation, 4 ms TR for each view, 1.3 s magnetization recovery time,[35] and in-plane Auto-calibrating Reconstruction for Cartesian Imaging (ARC) acceleration[48] by a factor of two. Afterwards, 2-echo MAPSS with one TSL and one TE_{eff} was performed by varying T_{prep} (= TSL = TE_{eff} - 1.2 ms) from 11.7 ms, 16.6 ms, 24.6 ms, to 37.4 ms using equivalent acquisition parameters.

In addition, B_0 field maps were measured using a 3D multi-echo gradient-echo sequence with prescribing 20 x 20 cm^2 FOV, 256 x 256 matrix size, 6 mm slice thickness, 16 slices, ±83.3 kHz readout bandwidth, 6.7 s TR, and TEs of 2.1/3.2/4.2/5.2/6.3/7.3 ms. B_0 field maps were automatically generated from the host computer using the iterative field map estimation method with region growing.[49,50] B_1 maps were acquired using the Bloch-Siegert shift method[51] incorporated to the 2D gradient-echo sequence with prescribing 16 x 16 cm^2 FOV, 128 x 128 matrix size, 10 mm slice thickness, 15 slices, 15° flip angle, 29 ms TR, and 12.4 ms TE.

From 8-echo MAPSS images, $T_{1\rho}$ and T_2 were estimated using the four echo signals through exponential curve fitting employing the Levenberg-Marquardt method,[52,53] and then reference R_2-$R_{1\rho}$ was obtained. From 2-echo MAPSS images, R_2-$R_{1\rho}$ was calculated using the difference between the negative logarithms of the signals divided by T_{prep}. ROIs with 4 cm^2 in area were located within each tube at four central slices, and the mean and standard deviation of R_2-$R_{1\rho}$ over the four ROIs of each tube were measured to compare R_2-$R_{1\rho}$ between different methods.

In Vivo Scan

In vivo validation was performed using a GE Discovery MR750 scanner (GE Healthcare, Waukesha, WI) and a 16-channel medium GEM flex-coil array (Neo-Coil, Pewaukee, WI). Five healthy subjects (age: 30.6 ± 7.4 years (mean ± STD), 4 males and 1 females) and five patients with OA (age: 54.8 ± 6.7 years, 3 males and 2 females) were studied after obtaining ethical approval and informed consent. Two of the patients with OA had a Kellgren–Lawrence (KL) grade[54] of 2, and the other three had a KL grade of 3, based on radiographs acquired within 6 months of each MRI exam.

For each subject, 7-echo MAPSS was first performed with TSLs of 0, 12.8, 40, 80 ms, and spin lock frequency of 500 Hz for $T_{1\rho}$ quantification, and TE_{eff} times of 0, 12.8, 25.7, and 51.4 ms for T_2 quantification. TSL = 0 images were shared as TE = 0 images for the in vivo study. Imaging parameters included were a FOV of 14 x 14 cm^2, 256 x 128 matrix size, 4 mm slice thickness, 22 slices, ±62.5 kHz readout bandwidth, 64 view acquisition per each $T_{1\rho}$ or T_2 preparation, 5.7 – 6.4 ms TR for each view, 1.3 s magnetization recovery time, and in-plane ARC acceleration by a factor of two, resulting in 9.8 min scan time. Afterwards, 2-echo MAPSS with one TSL and one TE was performed by varying the TSL and TE_{eff} from 12.8 ms, 17.7 ms, 25.7 ms, to 38.5 ms using equivalent acquisition parameters (T_2-prepared images were acquired at a 1.2 ms lower T_{prep} than $T_{1\rho}$-prepared images). Each 2-echo MAPSS required 2.8 - 3 min scan time. For five out of the ten subjects, B_0 field maps and B_1 maps were acquired employing the mapping sequences used for the phantom study to assess B_0 and B_1 variations within cartilages, to determine the reliability of the 2-echo MAPSS method in quantifying in vivo knee cartilage.

In Vivo Data Post Processing and Quantification

Rigid registration between different TSL/TE images for each MAPSS data set was first applied when echo-to-echo spatial displacement was observed. From 7-echo MAPSS images, $T_{1\rho}$ and T_2 were estimated using the four echo signals and then reference R_2-$R_{1\rho}$ was obtained. For 2-echo MAPSS, T_2-prepared signals was scaled by 0.97 to compensate acquisition at 1.2 ms lower T_{prep} than $T_{1\rho}$ -prepared signals assuming a cartilage T_2 of 36 ms (between the mean values of healthy subjects and osteoarthritis patients[55]). Then R_2-$R_{1\rho}$ was calculated using the difference between the negative logarithms of the signals divided by T_{prep}.

Cartilage was segmented semi-automatically using in-house developed software based on edge detection and Bezier splines.[56] Cartilage was divided into six different compartments, medial femoral condyle/tibia (MFC/MT), lateral femoral condyle/tibia (LFC/LT), lateral femoral trochlea (TrF), and patella (PT), with each compartment segmented on 4-8 slices of the second-TSL images of 7-echo MAPSS data. Fluid was excluded by exploiting the fourth-TSL images. For each 2-echo MAPSS data set, segmented regions were manually adjusted to correct for subject motion. The mean R_2-$R_{1\rho}$ values were computed for each compartment over the ten subjects. Correlation and Bland-Altman analysis were performed to compare conventional and efficient R_2-$R_{1\rho}$ quantification methods. Statistical difference in R_2-$R_{1\rho}$ (by 7-echo MAPSS) for each cartilage compartment was assessed between the healthy subjects and patients using the Wilcoxon rank-sum test.

To assess B_0 and B_1 variations within cartilage regions, B_0 field maps and B_1 maps were resampled to match the FOV and pixel size of MAPSS images. The distribution of B_0 off-resonance frequencies and relative B_1 (the measured flip angle divided by the nominal flip angle) within the six segmented cartilage compartments were assessed over the five subjects.

Results

Simulation

Simulated signal magnitudes after $T_{1\rho}$ and T_2 preparation with varying T_{prep} and derived R_2-$R_{1\rho}$ are shown in Figure 2. Tissue relaxation times of T_2 = 33 ms, $T_{1\rho}$ = 43 ms, and T_1 = 1.2 s were used, and B_0 and B_1 inhomogeneities were assumed not to be present. Noise was added to yield an SNR from 125 to 50 when T_{prep} = 0 on each coil image. Simulations indicated decrease in SNR yielded an increased signal bias in the signal magnitude, and R_2-$R_{1\rho}$ was further deviated from the reference. T_{prep} that could provide R_2-$R_{1\rho}$ closest to the reference was also affected by SNR.

Figure 3A, B illustrates $T_{1\rho}$- and T_2-prepared signals and resulted R_2-$R_{1\rho}$ over T_{prep} variation for five different combinations of T_2 and $T_{1\rho}$ relaxation times. SNR in coil images was assumed to be 100 when T_{prep}= 0, close to the measurement from in vivo knee MAPSS images (when using the 16-channel medium flex-coil array). The optimal T_{prep} increased with higher relaxation times, but overall, T_{prep} around 25 ms provided R_2-$R_{1\rho}$ close to the reference. Figure 3C shows the simulated R_2-$R_{1\rho}$ values subtracted by the reference (calculated from applied T_2 and $T_{1\rho}$ values) over a B_0 offset from −250 to 250 Hz and a relative B_1 from 0.7 to 1.3, when T_{prep} = 24.5 ms. This T_{prep} provided a difference around -8 s^{-1} when $T_2/T_{1\rho}$ = 10/15 ms, but with higher relaxation times, the difference was close to 0 within off-resonances of ±100 Hz and relative B_1 variations of 0.9 - 1.1.

Phantom Study

$T_{1\rho}$, T_2, and R_2-$R_{1\rho}$ maps of the agarose phantoms using 8-echo MAPSS are shown in Figure 4D, and E. $T_{1\rho}$ and T_2 ranged between 15 ms and 75 ms over five different concentrations, decreased with increased agarose concentration as expected.[46] The difference between $T_{1\rho}$ and T_2 was very small, but we can still observe increase of R_2-$R_{1\rho}$ with agarose concentration, probably indicating increased chemical exchange. Figure 4F shows R_2-$R_{1\rho}$ maps based on 2-echo MAPSS at the four different T_{prep} times. Increase of R_2-$R_{1\rho}$ with concentration was well depicted although variations of B_0 off-resonance and relative B_1 (Figure 4B,C) seemed to affect homogeneity of R_2-$R_{1\rho}$ within each tube. For example, increased R_2-$R_{1\rho}$ due to a large B_0 offset was visible in the tube with 6% concentration (depicted by arrows). Based on ROI analysis (4 ROIs for each tube), T_{prep} = 24.5 ms provided the minimum bias in the means (0.13 s^{-1}) compared to those from reference, and the minimum mean standard deviation over the tubes. Figure 4H compares the mean and standard deviation of R_2-$R_{1\rho}$ within each tube between 8-echo MAPSS and 2-echo MAPSS at T_{prep} = 24.5 ms. The mean values were very similar between the two methods for the agarose phantoms with concentrations of 4, 6, and 8% (within a difference of 0.05 s^{-1}) while 2-echo MAPSS yielded higher standard deviations.

In Vivo Study

Quantification results from one representative healthy subject are shown in Figure 5. Figure 5A,C shows $T_{1\rho}$, T_2, and R_2-$R_{1\rho}$ maps at two different slice locations from 7-echo MAPSS, and Figure 5B,D shows R_2-$R_{1\rho}$ maps from 2-echo MAPSS with four different T_{prep} values at the matching locations. The deep layers, which include highly organized collagen fibers,[11]

had relatively shorter $T_{1\rho}$ and T_2 and higher R_2-$R_{1\rho}$ compared to the superficial layers. Figure 5E depicts acquired signals and derived R_2-$R_{1\rho}$ with 2-echo MAPSS at the four T_{prep} times from the pixels located in MFC, MT, PT, and LFC. $T_{1\rho}$ and T_2 decay curves and reference R_2-R_1 based on fitted $T_{1\rho}$ and T_2 from 7-echo MAPSS are denoted as dashed lines as well. R_2-$R_{1\rho}$ was estimated close to the reference using 2-echo MAPSS. However, we can check that for the pixel with high R_2-$R_{1\rho}$ (pixel 2), using a long T_{prep} yielded a larger error. In contrast, for the pixel with small R_2-$R_{1\rho}$ (pixel 4), 2-echo MAPSS with a short T_{prep} yielded a larger error.

Results from two patients are illustrated in Figure 6 with again $T_{1\rho}$, T_2, and R_2-$R_{1\rho}$ maps from 7-echo MAPSS as well as R_2-$R_{1\rho}$ maps from 2-echo MAPPS. Overall, elevated $T_{1\rho}$ and T_2 values and lower R_2-$R_{1\rho}$ values were seen compared to the healthy subjects. R_2-$R_{1\rho}$ maps from 2-echo MAPSS depicted patterns similar to what from 7-echo MAPSS.

Figure 7 compares the mean R_2-$R_{1\rho}$ values of the six different cartilage compartments for each subject between 7-echo MAPSS and 2-echo MAPSS. Scatter plots (Figure 7A) demonstrated a strong correlation between the two measurements; when T_{prep} = 25.7 ms, the correlation of determination was the highest (r^2 = 0.78). The Bland-Altman plots (Figure 7B) also demonstrated that T_{prep} = 25.7 ms provided a bias close to 0 and the coefficient of variance (the ratio between the standard deviation of each difference and the average of each mean) was smaller (13%) than other T_{prep} values. The mean R_2-$R_{1\rho}$ values (based on 7-echo data) were statistically lower in patients than in healthy subjects for all compartments except MT based on the Wilcoxon rank-sum test ($P < 0.05$).

There existed B_0 and B_1 variations over the imaging volume. In particular, Figure 8 shows B_0 field maps and relative B_1 maps at the medial and lateral slices from a healthy subject. However, we were able to see that variations within cartilage regions were not that significant. Figure 8G-H shows histograms of B_0 off-resonance frequencies and relative B_1 values within the six cartilage compartments over the five subjects. The central 80% of B_0 off-resonance frequencies were within the range from −38 to 5 Hz, and 80% of relative B_1 values were within the range from 0.88 to 1.19. These B_0 and B_1 variations can provide R_2-$R_{1\rho}$ close to the actual value based on Bloch equation simulations (Figure 3C).

Discussion

In this work, we demonstrated that R_2-$R_{1\rho}$ quantification from 2-echo MAPSS shows a good agreement with those from 7-echo MAPSS. Our Bloch equation simulations demonstrated that careful selection of T_{prep} will allow for R_2-$R_{1\rho}$ quantification not much affected by image noise over a wide range of possible relaxation times for cartilage. Our in vivo results from ten subjects also revealed that T_{prep} of 25.7 ms provided quantification results most similar to those from the conventional method.

Derivation of R_2-$R_{1\rho}$ from 2-echo MAPSS signals assumes that $S_{1\rho}(0)$ and $S_2(0)$ are equivalent. To achieve this, careful comparison between $T_{1\rho}$ and T_2 preparation is needed. Designating T_{prep} as TSL for $T_{1\rho}$ preparation and T_{prep} as TE_{eff}, which results in TSL = TE_{eff}, would provide a lower $S_{1\rho}(0)$ than $S_2(0)$ because of additional relaxation with $T_{1\rho}$

preparation happening during the two 135° hard pulses for the composite tip-down and tip-up pulses. By approximating the relaxation time constant during these RF pulses as T_2, setting T_{prep} as TE_{eff} subtracted by the two 135° hard pulse duration for T_2 preparation, i.e., $T_{prep} = TE_{eff} - 2*T_{RF135}$, will provide $S_{1\rho}(0)$ and $S_2(0)$ more similar. Our simulations and phantom study used $T_{prep} = TE_{eff} - 2*T_{RF135}$ for 2-echo MAPSS acquisition, but our in vivo study was performed with TSL = TE_{eff}. To mimic T_{prep} of $TE_{eff} - 2*T_{RF135}$ for T_2-prepared signal, the acquired T_2-prepared signal was multiplied by 0.97 assuming a T_2 of 36 ms. This scaling might have resulted in a higher R_2-$R_{1\rho}$ for regions with T_2 >36 ms and a lower R_2-$R_{1\rho}$ for regions with T_2 < 36 ms. If actual in vivo acquisition had been performed with the proposed T_{prep}, R_2-$R_{1\rho}$ quantification with 2-echo MAPSS might have been improved. Another concern is that TE_{eff} might not be estimated correctly when the assumption of T_1 over T_2 as 34 is not suitable due to cartilage degeneration. T_1 might not vary much (reported as 1.2 s at 3T[40]), but T_2 might vary[55] over 15 - 70 ms. However, even the actual T_1/T_2 varies over 20-50, the error in TE_{eff} by assuming T_1/T_2 as 34 would be between −0.25% and 0.37%.

The use of composite RF pulses and phase cycling for $T_{1\rho}$ preparation is effective in reducing B_0 and B_1 inhomogeneity effects, and these approaches can minimize errors in R_2-$R_{1\rho}$ quantification when using the direct subtraction between the logarithms of acquired signals. Chen et al.[38] demonstrated the effectiveness of this $T_{1\rho}$-preparation scheme to correct B_0 and B_1 inhomogeneity effects in comparison to other frequently-used techniques. For our phantom study, B_0 off-resonance variation existed within each tube due to its cylindrical shape, up to 60 Hz variation along the diameter (2.5 cm), and these inhomogeneity effects were noticeable in R_2-$R_{1\rho}$ quantification. However, for the in vivo study, we measured B_0 off-resonances of −38 - 5 Hz and relative B_1 variations of 0.88 - 1.19 for 80% of total cartilage pixels (over five subjects), and thus inhomogeneity effects on R_2-$R_{1\rho}$ would not be that significant as simulations verified.

Our phantom study depicted increase in R_2-$R_{1\rho}$ with agarose gel concentration, possibly indicating higher chemical exchange between free water and macromolecule. However, the value was small, under 2 s^{-1} even with 10% concentration. Li et al[46] previously reported no observable dispersion between spin lock frequency of 150 Hz and 1000 Hz in agarose gel phantoms. We measured the negative R_2-$R_{1\rho}$ with 2% gel concentration, and it might have resulted from inaccurate TE_{eff} calculation, inhomogeneity effects, or nonoptimal sets of TE_{eff} values to estimate 75 ms T_2 accurately.

Our sample size was small (five healthy subjects and five patients); though R_2-$R_{1\rho}$ in the patient group was statistically lower than the healthy subject group for five out of six compartments, supporting previous results on the potential utility of R_2-$R_{1\rho}$ as OA imaging biomarker.[34] Assessing patients with various stages of OA will allow for further evaluation of clinical utility in R_2-$R_{1\rho}$. R_2 and $R_{1\rho}$ had a relaxation component describing dipolar interactions as well as a component resulted from chemical exchange between hydroxyl (−OH) protons in bulk water and in PG.[32,57] With the increase in the spin lock frequency (w_1), the relaxation rate contributed from dipolar interaction reduces based on molecular rotation correlation time (γ_c), described by an equation of $R_{1\rho}{}^{DD} \propto 1.5\gamma_c / (1 + 4w_1^2\gamma_c^2) + K$,

where γ_c depends on surrounding macrostructure (increased with tighter collagen structure) and K depends on B_0 resonant frequency and γ_c. In addition, the relaxation rate contributed from chemical exchange between bulk water and PG also reduces with the spin lock frequency based on chemical exchange rate (r^{ex}) and fractional population of bulk water and PG pools (p_a, p_b), described by an equation of $R_{1\rho}{}^{ex} = \delta^2 p_a p_b r_{ex} / (w_1^2 + r_{ex}^2 + \delta^2)$, where δ is the chemical shift frequency of (−OH) protons in PG.[58,59] Therefore, $R_{1\rho}$ difference between the two spin lock frequencies (0 and 500 Hz) can be a metric associated with γ_c, p_b, *and* r_{ex}, and can characterize ECM better than either R_2 or R_1.[31,60] Small $R_{1\rho}$ difference might reflect either reduced collagen integrity (represented by decreased γ_c) or reduced chemical exchange effect (decreased p_b or r_{ex}), either of which results from cartilage degeneration. Alternatively, different spin lock frequencies might be employed if they can characterize ECM better. Previously, Wang et al[60] used 100 and 350 Hz spin lock frequencies in calculating $R_{1\rho}$ difference to represent dispersion curves.

Articular cartilage collagen structure is more organized in deep layers than in superficial layers, thus deep layers exhibit R_2-$R_{1\rho}$ higher than superficial layers for healthy subjects. In addition, deep layers contain higher concentration of PG,[4] which might enhance R_2-$R_{1\rho}$. Because of their inherent structural, compositional variations within cartilage, separate quantification of the superficial and deep layers might better delineate change due to degeneration:[30,61] division into three layers of superficial, transitional, and deep layers is difficult considering spatial resolution with in vivo imaging. R_2-$R_{1\rho}$ is also still sensitive to magic angle effects like T_2 and $T_{1\rho}$[13,62,63] since relaxation due to dipolar interaction has orientation dependance based on the angle between the collagen fiber direction and the main magnetic field.[64] Therefore, the magic angle effects need to be considered when assessing R_2-$R_{1\rho}$ for detecting cartilage degeneration.

There are several limitations on this efficient method and our imaging parameters to address. Because efficient R_2-$R_{1\rho}$ measurement uses only two pixel signals for quantification, this method can be highly sensitive to spatial misregistration between the two image sets. Perfect alignment is critical for accurate quantification. In addition, any artifacts perturbing original cartilage signals such as flow artifacts will also directly affect quantification. However, since flow artifacts from MAPSS mostly affects posterior regions of LFC, the presence of flow artifacts can be evaluated from acquired MAPSS images and affected regions can be excluded during analysis. In addition, the SNR in R_2-$R_{1\rho}$ maps can be also lower than the conventional method, so there should be sufficient SNR for each echo image to use this efficient method. As for our imaging parameters, the slice thickness of 4 mm can be large for knee cartilage assessment, and cartilage quantification can be affected by partial volume effects, in particular, in cartilage regions adjacent to synovial fluid or bone. However, we believe this efficient approach might be exploited to improve spatial resolution for knee cartilage assessment without the need of a long scan time as far as the SNR is sufficient. Another limitation of this current approach is the optimal T_{prep} might vary depending on image SNR. However, it might be possible the estimate original signal resulted from magnetization by estimating noise standard deviation from background ROI and correcting signal bias.[44] This can provide 2-echo MAPSS R_2-$R_{1\rho}$ quantification less affected by the SNR.

This efficient R_2-$R_{1\rho}$ quantification method has a high potential to delineate cartilage degeneration with a very short acquisition time. We have only applied this technique for knee cartilage, but the same approach can be used for hip cartilage though B_0 and B_1 inhomogeneity effects can be higher. This method can be also applied to assess other connective tissues such as tendons, menisci, and ligaments, which also consist of ECM primarily containing collagen, PG, and water.

Conclusions

We have demonstrated that knee cartilage R_2-$R_{1\rho}$ can be quantified using one pair of $T_{1\rho}$-weighted signal and T_2-weighted signal while reducing acquisition time by 70% compared to the conventional method that respectively fitted T_2 and $T_{1\rho}$ (acquisition time from 10 mins to 3 mins for one knee). A preparation time of 25.6 ms provided the most correlated and agreeable R_2-$R_{1\rho}$ in knee cartilage to that of the conventional method. R_2-$R_{1\rho}$ was significantly lower in patients than in healthy subjects, demonstrating a high potential to provide information pertaining to cartilage ECM change associated with degeneration.

Acknowledgements

The authors would like to thank Dr. Michael Carl for help to modify MAPSS pulse sequence programs with scanner software upgrade, Dr. Roland Krug for allowing for using agarose phantoms for the phantom study, Dr. Upasana Bharadwaj for assessing radiography of patients to provide KL grades, and Dr. Peder Larson and Dr. Weitian Chen for helpful discussion about this project. This work was supported by NIH/NIAMS R01AR069006 and NIH/NIAMS K01AR075895.

References

1. Lawrence RC, Felson DT, Helmick CG, et al. Estimates of the prevalence of arthritis and other rheumatic conditions in the United States. Part II. Arthritis Rheum. 2008;58(1):26–35. [PubMed: 18163497]
2. Neogi T, Zhang Y. Epidemiology of osteoarthritis. Rheum Dis Clin North Am. 2013;39(1):1–19. [PubMed: 23312408]
3. Bollet AJ, Nance JL. Biochemical Findings in Normal and Osteoarthritic Articular Cartilage. II. Chondroitin Sulfate Concentration and Chain Length, Water, and Ash Content. J Clin Invest. 1966;45(7):1170–1177. [PubMed: 16695915]
4. Venn M, Maroudas A. Chemical composition and swelling of normal and osteoarthrotic femoral head cartilage. I. Chemical composition. Ann Rheum Dis. 1977;36(2):121–129. [PubMed: 856064]
5. Sophia Fox AJ, Bedi A, Rodeo SA. The basic science of articular cartilage: structure, composition, and function. Sports Health. 2009;1(6):461–468. [PubMed: 23015907]
6. Buckwalter JA, Mankin HJ, Grodzinsky AJ. Articular cartilage and osteoarthritis. Instr Course Lect. 2005;54:465–480. [PubMed: 15952258]
7. Carney SL, Muir H. The structure and function of cartilage proteoglycans. Physiol Rev. 1988;68(3):858–910. [PubMed: 3293094]
8. Lane JM, Weiss C. Review of articular cartilage collagen research. Arthritis Rheum. 1975;18(6):553–562. [PubMed: 173345]
9. Buckwalter J, Mankin H. Articular cartilage: part I. J Bone Jt Surg. 1997;79(4):600.
10. Pearle AD, Warren RF, Rodeo SA. Basic science of articular cartilage and osteoarthritis. Clin Sports Med. 2005;24(1):1–12. [PubMed: 15636773]
11. Dijkgraaf LC, de Bont LG, Boering G, Liem RS. The structure, biochemistry, and metabolism of osteoarthritic cartilage: a review of the literature. J Oral Maxillofac Surg. 1995;53(10):1182–1192. [PubMed: 7562173]

12. Kraus VB. Pathogenesis and treatment of osteoarthritis. Med Clin North Am. 1997;81(1):85–112. [PubMed: 9012756]
13. Xia Y, Farquhar T, Burton-Wurster N, Lust G. Origin of cartilage laminae in MRI. J Magn Reson Imaging. 1997;7(5):887–894. [PubMed: 9307916]
14. Nieminen MT, Toyras J, Rieppo J, et al. Quantitative MR microscopy of enzymatically degraded articular cartilage. Magn Reson Med. 2000;43(5):676–681. [PubMed: 10800032]
15. Mosher TJ, Dardzinski BJ, Smith MB. Human articular cartilage: influence of aging and early symptomatic degeneration on the spatial variation of T2--preliminary findings at 3 T. Radiology. 2000;214(1):259–266. [PubMed: 10644134]
16. Akella SVS, Regatte RR, Wheaton AJ, Borthakur A, Reddy R. Reduction of residual dipolar interaction in cartilage by spin-lock technique. Magn Reson Med. 2004;52(5):1103–1109. [PubMed: 15508163]
17. Duvvuri U, Reddy R, Patel SD, Kaufman JH, Kneeland JB, Leigh JS. T1ρ-relaxation in articular cartilage: effects of enzymatic degradation. Magn Reson Med. 1997;38(6):863–867. [PubMed: 9402184]
18. Akella SV, Regatte RR, Gougoutas AJ, et al. Proteoglycan-induced changes in T1rho-relaxation of articular cartilage at 4T. Magn Reson Med. 2001;46(3):419–423. [PubMed: 11550230]
19. Regatte RR, Akella SVS, Borthakur A, Reddy R. Proton spin-lock ratio imaging for quantitation of glycosaminoglycans in articular cartilage. J Magn Reson Imaging. 2002;17(1):114–121.
20. Mlynarik V, Trattnig S, Huber M, Zembsch A, Imhof H. The role of relaxation times in monitoring proteoglycan depletion in articular cartilage. J Magn Reson Imaging. 1999;10(4):497–502. [PubMed: 10508315]
21. Menezes NM, Gray ML, Hartke JR, Burstein D. T2 and T1ρ MRI in articular cartilage systems. Magn Reson Med. 2004;51(3):503–509. [PubMed: 15004791]
22. Ward KM, Aletras AH, Balaban RS. A new class of contrast agents for MRI based on proton chemical exchange dependent saturation transfer (CEST). J Magn Reson. 2000;143(1):79–87. [PubMed: 10698648]
23. Ling W, Regatte RR, Navon G, Jerschow A. Assessment of glycosaminoglycan concentration in vivo by chemical exchange-dependent saturation transfer (gagCEST). Proc Natl Acad Sci U S A. 2008;105(7):2266–2270. [PubMed: 18268341]
24. Singh A, Haris M, Cai K, et al. Chemical exchange saturation transfer magnetic resonance imaging of human knee cartilage at 3 T and 7 T. Magn Reson Med. 2012;68(2):588–594. [PubMed: 22213239]
25. Chopra S, McClung R, Jordan R. Rotating-frame relaxation rates of solvent molecules in solutions of paramagnetic ions undergoing solvent exchange. J Magn Reson. 1984;59(3):361–372.
26. Cobb JG, Xie J, Gore JC. Contributions of chemical exchange to T1ρ dispersion in a tissue model. Magn Reson Med. 2011;66(6):1563–1571. [PubMed: 21590720]
27. Makela HI, Grohn OH, Kettunen MI, Kauppinen RA. Proton exchange as a relaxation mechanism for T1 in the rotating frame in native and immobilized protein solutions. Biochem Biophys Res Commun. 2001;289(4):813–818. [PubMed: 11735118]
28. Duvvuri U, Goldberg AD, Kranz JK, et al. Water magnetic relaxation dispersion in biological systems: the contribution of proton exchange and implications for the noninvasive detection of cartilage degradation. Proc Natl Acad Sci U S A. 2001;98(22):12479–12484. [PubMed: 11606754]
29. Mlynarik V, Szomolanyi P, Toffanin R, Vittur F, Trattnig S. Transverse relaxation mechanisms in articular cartilage. J Magn Reson. 2004;169(2):300–307. [PubMed: 15261626]
30. Pang Y An order parameter without magic angle effect (OPTIMA) derived from dispersion in ordered tissue. Magn Reson Med. 2019;83(5):1783–1795. [PubMed: 31691348]
31. Kogan F, Singh A, Cai K, Haris M, Hariharan H, Reddy R. Investigation of chemical exchange at intermediate exchange rates using a combination of chemical exchange saturation transfer (CEST) and spin-locking methods (CESTrho). Magn Reson Med. 2011;68(1):107–119. [PubMed: 22009759]
32. Wang P, Zhu H, Kang H, Gore JC. R1ρ dispersion and sodium imaging in human calf muscle. Magn Reson Imaging. 2017;42:139–143. [PubMed: 28751202]

33. Russell C, Pedoia V, Majumdar S, Consortium A-A. Composite metric R2 − R1ρ (1/ T2 − 1/ T1ρ) as a potential MR imaging biomarker associated with changes in pain after ACL reconstruction: A six-month follow-up. J Orthop Res. 2016;35(3):718–729. [PubMed: 27563836]
34. Pedoia V, Haefeli J, Morioka K, et al. MRI and biomechanics multidimensional data analysis reveals R 2-R1ρ as an early predictor of cartilage lesion progression in knee osteoarthritis. J Magn Reson Imaging. 2017;47(1):78–90. [PubMed: 28471543]
35. Li X, Han ET, Busse RF, Majumdar S. In vivo T1ρ mapping in cartilage using 3D magnetization-prepared angle-modulated partitioned k-space spoiled gradient echo snapshots (3D MAPSS). Magn Reson Med. 2008;59(2):298–307. [PubMed: 18228578]
36. Li X, Wyatt C, Rivoire J, et al. Simultaneous Acquisition of T1ρ and T2 Quantification in Knee Cartilage: Repeatability and Diurnal Variation. J Magn Reson Imaging. 2014;39:1287–1293. [PubMed: 23897756]
37. Dixon WT, Oshinski JN, Trudeau JD, Arnold BC, Pettigrew RI. Myocardial suppression in vivo by spin locking with composite pulses. Magn Reson Med. 1996;36(1):90–94. [PubMed: 8795026]
38. Chen W, Takahashi A, Han E. Quantitative T1ρ imaging using phase cycling for B0 and B1 field inhomogeneity compensation. Magn Reson Imaging. 2011;29(5):608–619. [PubMed: 21524869]
39. Foltz WD, Stainsby JA, Wright GA. T2 Accuracy on a Whole-Body Imager. Magn Reson Med. 1997;38:759–768. [PubMed: 9358450]
40. Gold GE, Parfitt AM, Han E, et al. Musculoskeletal MRI at 3.0 T: relaxation times and image contrast. AJR Am J Roentgenol. 2004;183(2):343–351. [PubMed: 15269023]
41. Witschey WR 2nd, Borthakur A, Elliott MA, et al. Artifacts in T1ρ-weighted imaging: compensation for B1 and B0 field imperfections. J Magn Reson. 2007;186(1):75–85. [PubMed: 17291799]
42. Solomon I Rotary Spin Echoes. Phys Rev Lett. 1959;2(7):301–302.
43. Henkelman RM. Measurement of signal intensities in the presence of noise in MR images. Med Phys. 1985;12(2):232–233. [PubMed: 4000083]
44. Constantinides CD, Atalar E, McVeigh ER. Signal-to-noise measurements in magnitude images from NMR phased arrays. Magn Reson Med. 1997;38(5):852–857. [PubMed: 9358462]
45. Mitchell MD, Kundel HL, Axel L, Joseph PM. Agarose as a tissue equivalent phantom material for NMR imaging. Magn Reson Imaging. 1986;4(3):263–266. [PubMed: 3669940]
46. Li X, Han ET, Ma CB, Link TM, Newitt DC, Majumdar S. In vivo 3T spiral imaging based multi-slice T1ρ mapping of knee cartilage in osteoarthritis. Magn Reson Med. 2005;54(4):929–936. [PubMed: 16155867]
47. Henkelman RM, Huang X, Xiang QS, Stanisz GJ, Swanson SD, Bronskill MJ. Quantitative interpretation of magnetization transfer. Magn Reson Med. 1993;29(6):759–766. [PubMed: 8350718]
48. Brau AC, Beatty PJ, Skare S, Bammer R. Comparison of reconstruction accuracy and efficiency among autocalibrating data-driven parallel imaging methods. Magn Reson Med. 2008;59(2):382–395. [PubMed: 18228603]
49. Reeder SB, Pineda AR, Wen Z, et al. Iterative decomposition of water and fat with echo asymmetry and least-squares estimation (IDEAL): application with fast spin-echo imaging. Magn Reson Med. 2005;54(3):636–644. [PubMed: 16092103]
50. Yu H, Shimakawa A, McKenzie CA, Brodsky E, Brittain JH, Reeder SB. Multiecho water-fat separation and simultaneous R2* estimation with multifrequency fat spectrum modeling. Magn Reson Med. 2008;60(5):1122–1134. [PubMed: 18956464]
51. Sacolick LI, Wiesinger F, Hancu I, Vogel MW. B1 mapping by Bloch-Siegert shift. Magn Reson Med. 2010;63(5):1315–1322. [PubMed: 20432302]
52. Levenberg K A method for the solution of certain non-linear problems in least squares. Quart Appl Math. 1944;2(2):164–168.
53. Marquardt DW. An algorithm for least-squares estimation of nonlinear parameters. J Soc Indust Appl Math. 1963;11(2):431–441.
54. Kellgren JH, Lawrence JS. Radiological assessment of osteo-arthrosis. Ann Rheum Dis. 1957;16(4):494–502. [PubMed: 13498604]

55. Li X, Ma CB, Link TM, et al. In vivo T1ρ and T2 mapping of articular cartilage in osteoarthritis of the knee using 3 T MRI. Osteoarthritis Cartilage. 2007;15(7):789–797. [PubMed: 17307365]
56. Carballido-Gamio J, Bauer JS, Stahl R, et al. Inter-subject comparison of MRI knee cartilage thickness. Med Image Anal. 2008;12(2):120–135. [PubMed: 17923429]
57. Borthakur A, Mellon E, Niyogi S, Witschey W, Kneeland JB, Reddy R. Sodium and T1ρ MRI for molecular and diagnostic imaging of articular cartilage. NMR Biomed. 2006;19(7):781–821. [PubMed: 17075961]
58. Davis DG, Perlman ME, London RE. Direct measurements of the dissociation-rate constant for inhibitor-enzyme complexes via the T1ρ and T2 (CPMG) methods. J Magn Reson B. 1994;104(3):266–275. [PubMed: 8069484]
59. Trott O, Palmer AGr. R1ρ relaxation outside of the fast-exchange limit. J Magn Reson. 2002;154(1):157–160. [PubMed: 11820837]
60. Wang P, Block J, Gore JC. Chemical exchange in knee cartilage assessed by R1ρ (1/T1ρ) dispersion at 3T. Magn Reson Imaging. 2015;33(1):38–42. [PubMed: 25093631]
61. Li X, Kuo D, Theologis A, et al. Cartilage in anterior cruciate ligament-reconstructed knees: MR imaging T1ρ and T2--initial experience with 1-year follow-up. Radiology. 2011;258(2):505–514. [PubMed: 21177392]
62. Grunder W, Wagner M, Werner A. MR-microscopic visualization of anisotropic internal cartilage structures using the magic angle technique. Magn Reson Med. 1998;39(3):376–382. [PubMed: 9498593]
63. Shao H, Pauli C, Li S, et al. Magic angle effect plays a major role in both T1ρ and T2 relaxation in articular cartilage. Osteoarthritis Cartilage. 2017;25(12):2022–2030. [PubMed: 28161394]
64. Xia Y Relaxation anisotropy in cartilage by NMR microscopy (muMRI) at 14-microm resolution. Magn Reson Med. 1998;39(6):941–949. [PubMed: 9621918]

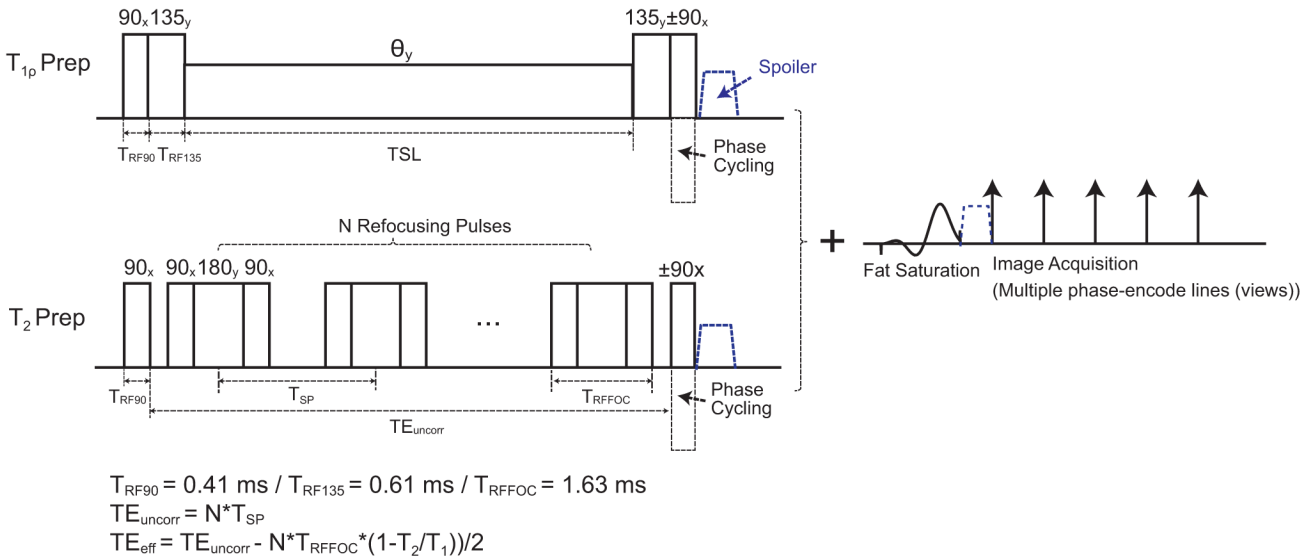

T_{RF90} = 0.41 ms / T_{RF135} = 0.61 ms / T_{RFFOC} = 1.63 ms
$TE_{uncorr} = N*T_{SP}$
$TE_{eff} = TE_{uncorr} - N*T_{RFFOC}*(1-T_2/T_1))/2$

Figure 1.

$T_{1ρ}$ and T_2 preparation incorporated to MAPSS. $T_{1ρ}$ preparation used composite tip-down and tip-up pulses while T_2 preparation used composite refocusing pulses with MLEV phase cycling. For each preparation, acquisitions were performed with ± signs of the 90° tip-up pulse and the subtraction of two acquired signals was used to be less sensitive to B_1 inhomogeneities (RF phase cycling). For T_2 preparation, TE was corrected (defined as TE_{eff}) based on the number of refocusing pulses, the duration of each refocusing pulses, and the ratio of T_1 and T_2. Multiple phase-encode lines (views) were acquired after each preparation.

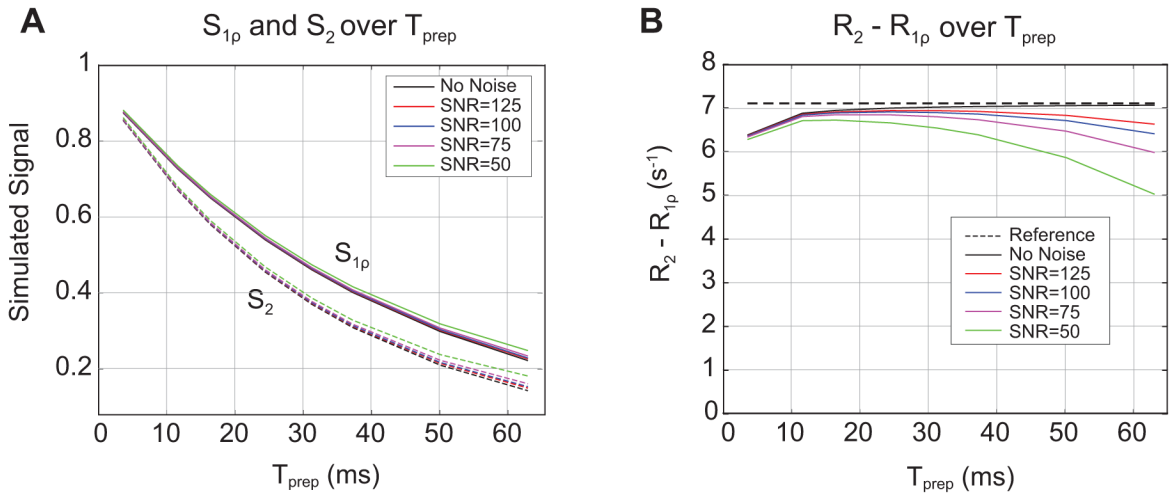

Figure 2.

Bloch equation simulations and noise effects. (A) $T_{1\rho}$- and T_2-prepared signals by varying the T_{prep} assuming T_2 = 33 ms and $T_{1\rho}$ = 43 ms. Noise was added assumed to yield SNR at each coil image from 125 to 50 when T_{prep} = 0. (B) Derived R_2-$R_{1\rho}$ based on $T_{1\rho}$- and T_2-prepared signals over the T_{prep}. Increased noise yields an increased signal bias and results in an increased error for R_2-$R_{1\rho}$ quantification.

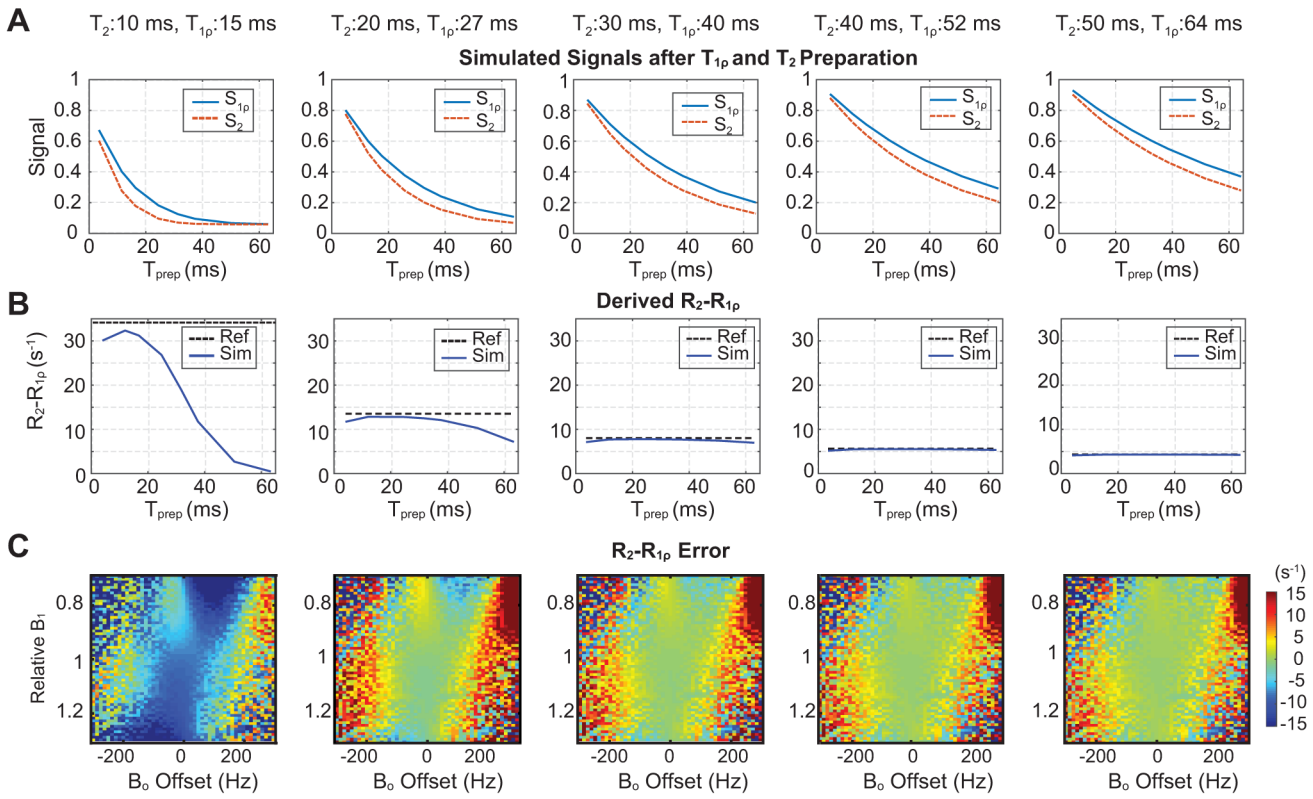

Figure 3.

Bloch equation simulations with various tissue relaxation times. (A) Simulated $T_{1\rho}$- and T_2-prepared signals over T_{prep}. Five different combinations of T_1 and T_2 relaxation times (within possible ranges in cartilage) were used, assuming the SNR over each coil image when T_{prep} = 0 was 100. (B) Derived R_2-$R_{1\rho}$ from simulated $T_{1\rho}$- and T_2-prepared signals compared to the reference. (C) R_2-$R_{1\rho}$ difference between simulation and the reference over a B_0 offset of −250 to 250 Hz and relative B_1 variation of 0.7 to 1.3 (T_{prep} was set to 25 ms). The difference is close to 0 within a B_0 offset of ±100 Hz and a relative B_1 variation of 0.9 - 1.1 except with the first pair of relaxation times.

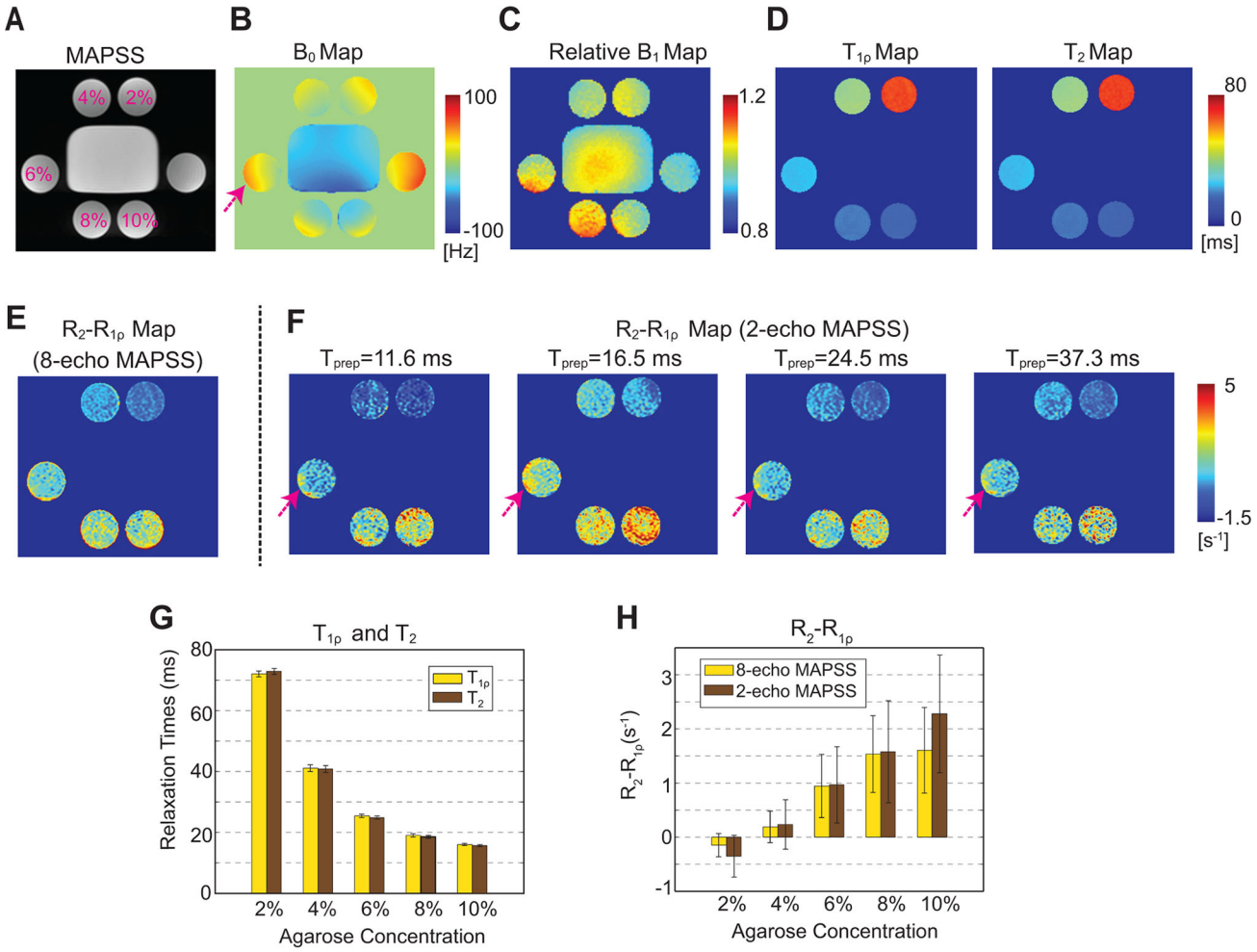

Figure 4.

Phantom study using agarose gel with concentration of 2 - 10%. (A) MAPSS images with TSL = 0. (B,C) B_0 field map and relative B_1 map (the measured flip angles over the nominal flip angle). (D,E) $T_{1\rho}$, T_2, and R_2-$R_{1\rho}$ maps fitted and derived from 8-echo MAPSS. $T_{1\rho}$ and T_2 decrease while R_2-$R_{1\rho}$ increases with increased agarose concentration. (F) R_2-$R_{1\rho}$ maps from 2-echo MAPSS acquired at the four different T_{prep} times. (G) The means and standard deviations of $T_{1\rho}$ and T_2 over four ROIs within each tube. (H) The means and standard deviations of R_2-$R_{1\rho}$ from 8-echo MAPSS and 2-echo MAPSS with T_{prep} of 24.48 ms. The standard deviations are higher with 2-echo MAPSS although the mean values are very similar between the two methods for tubes with concentrations of 4,6, and 8%.

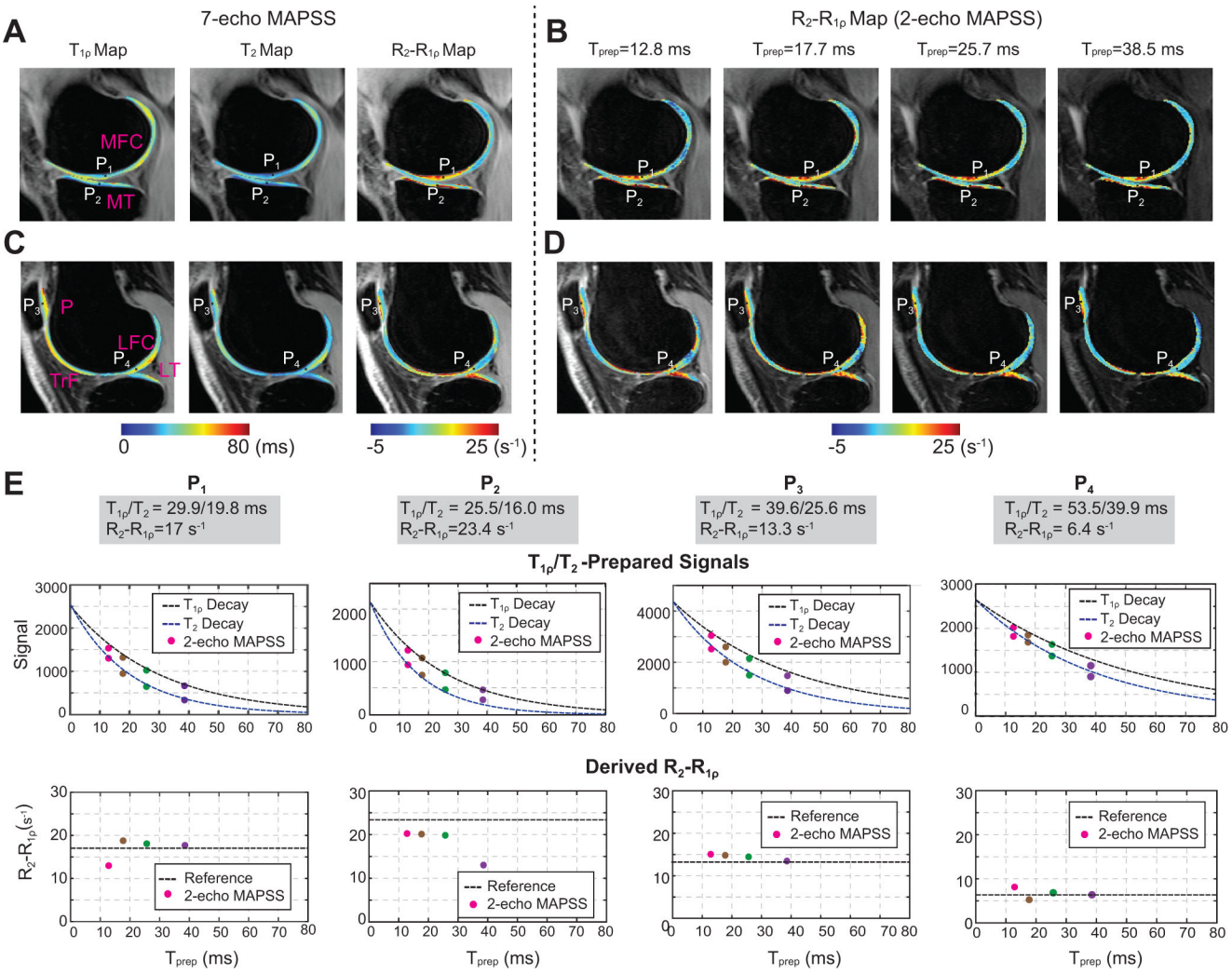

Figure 5.

Healthy subject results. (A,C) $T_{1\rho}$, T_2, and R_2-$R_{1\rho}$ maps from 7-echo MAPSS at two different slice locations. (B,D) R_2-$R_{1\rho}$ maps from 2-echo MAPSS with four different T_{prep} at the matching locations. The deep layers exhibit shorter $T_{1\rho}$ and T_2 and higher R_2-$R_{1\rho}$ compared to the superficial layers. (E) These plots depict measured signals (after compensation for T_2-prepared signals) and derived R_2-$R_{1\rho}$ with 2-echo MAPSS at the four T_{prep} times (different colors for different 2-echo MAPSS scans). The locations of pixels 1 - 4 (P_1 - P_4) are depicted in (A-D). Estimated $T_{1\rho}$, T_2, and R_2-$R_{1\rho}$ from 7-echo MAPSS are denoted above the plots, and corresponding $T_{1\rho}$ and T_2 decay curves and reference R_2-$R_{1\rho}$ are depicted as dashed lines in these plots.

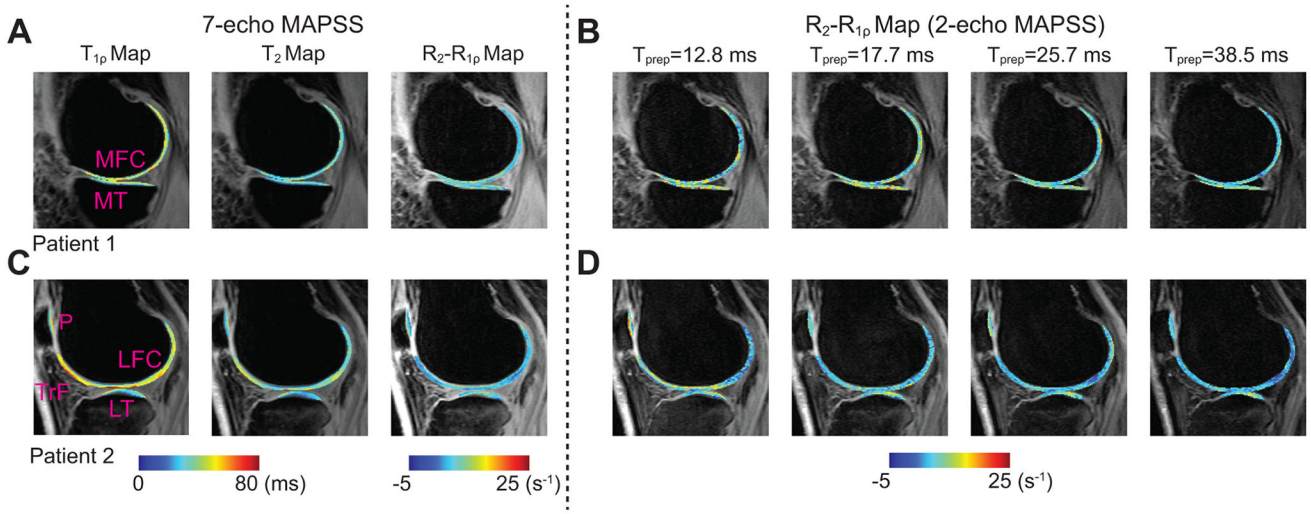

Figure 6.

Patient results. (A,C) $T_{1\rho}$, T_2, and R_2-$R_{1\rho}$ maps by 7-echo MAPSS from two patients. (B,D) R_2-$R_{1\rho}$ maps from 2-echo MAPPS at the matching slices. Increased $T_{1\rho}$ and T_2 and decreased R_2-$R_{1\rho}$ values are observed, compared to the previous healthy subject. R_2-$R_{1\rho}$ maps from 2-echo MAPSS exhibit patterns similar to what from 7-echo MAPSS.

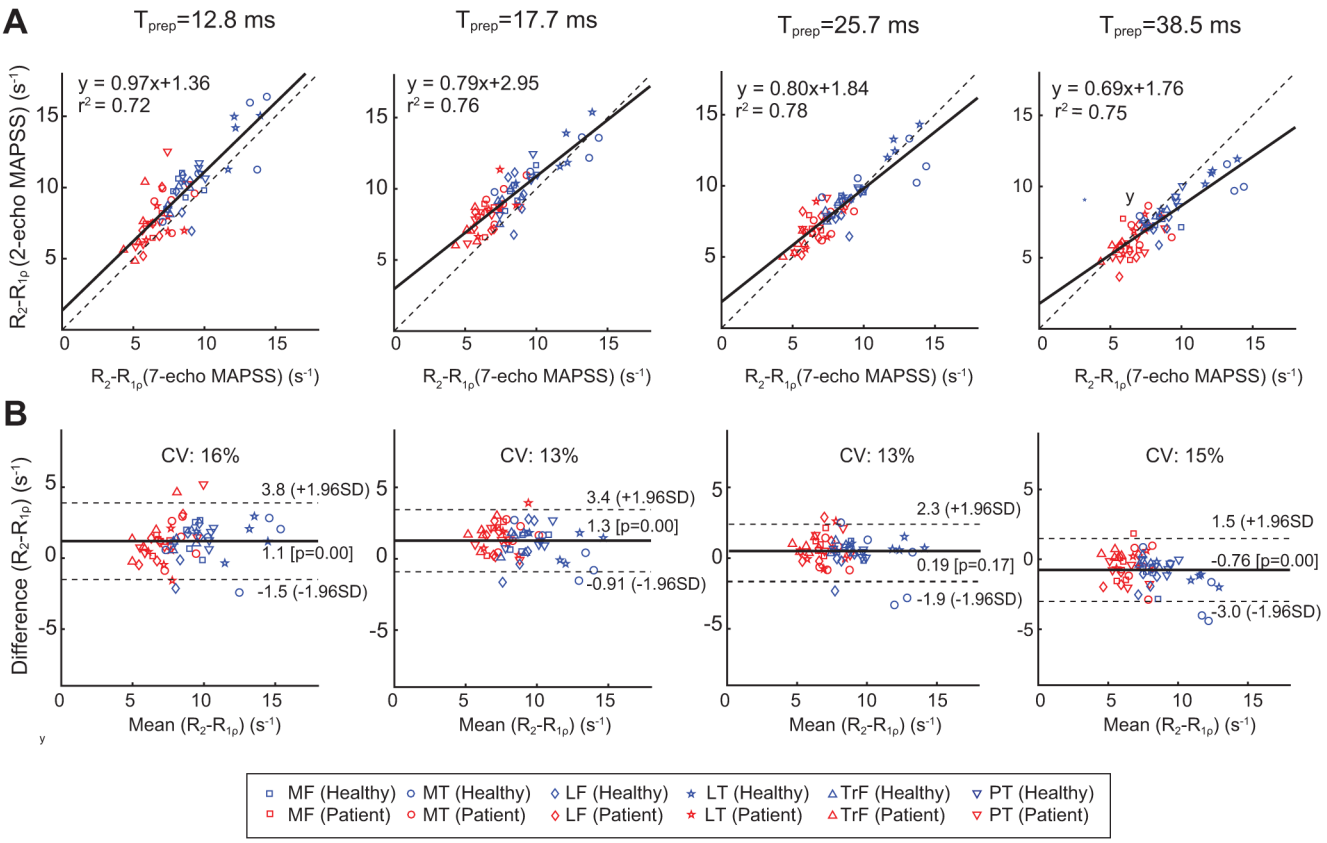

Figure 7.

Average R_2-$R_{1\rho}$ for each cartilage compartment from the ten subjects measured 7-echo and 2-echo MAPSS. (A) Scatter plots to assess correlation in R_2-$R_{1\rho}$ between the two methods at four different T_{prep} times. (B) Bland-Altman plots to assess agreement between the two methods. Scatter plots and Bland-Altman plots show that T_{prep} = 25.7 ms can provide the most agreeable quantification results between 7-echo and 2-echo MAPSS with the minimum coefficient of variance (CV).

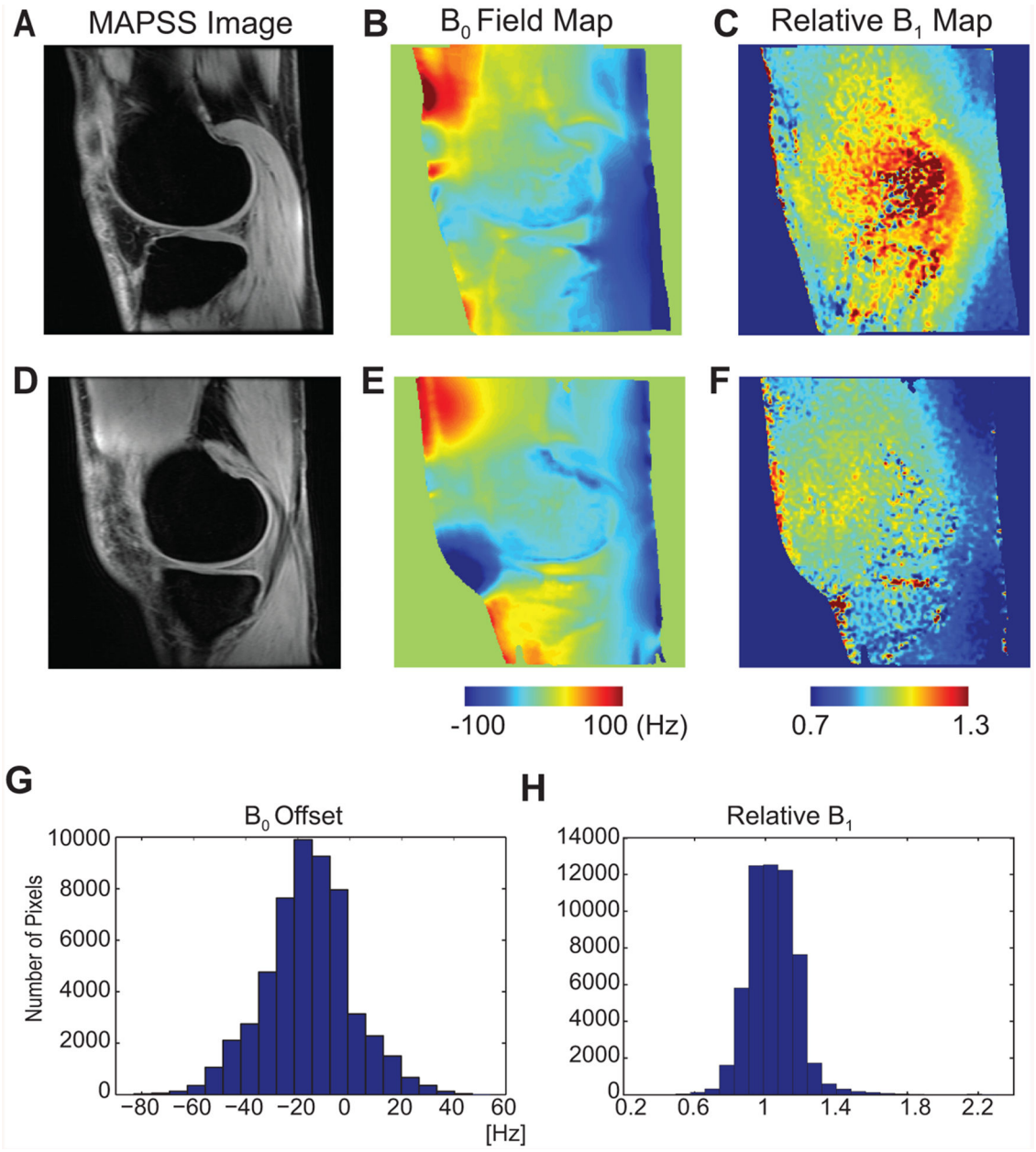

Figure 8.

B_0 and B_1 inhomogeneities in knee cartilage. (A-F) MAPSS TSL = 0 images, and B_0 field maps and relative B_1 maps at two different slices from one healthy subject. B_0 and B_1 variations within each slice can be seen. (G-H) Histograms of B_0 off-resonance frequencies and relative B_1 variations over the six compartments of five subjects.